Integrated Systems and Technologies

Cancer Research

Unexpected Dissemination Patterns in Lymphoma Progression Revealed by Serial Imaging within a Murine Lymph Node

Ken Ito[1,2], Bryan Ronain Smith[1,2], Natesh Parashurama[1,2], Joon-Kee Yoon[1,2,4], Si Yeol Song[1,2,5], Cornelius Miething[3], Parag Mallick[1,2], Scott Lowe[3], and Sanjiv Sam Gambhir[1,2]

Abstract

Non-Hodgkin lymphoma (NHL) is a heterogeneous and highly disseminated disease, but the mechanisms of its growth and dissemination are not well understood. Using a mouse model of this disease, we used multimodal imaging, including intravital microscopy (IVM) combined with bioluminescence, as a powerful tool to better elucidate NHL progression. We injected enhanced green fluorescent protein and luciferase-expressing Eμ-Myc/Arf$^{-/-}$ (Cdkn2a$^{-/-}$) mouse lymphoma cells (EL-Arf$^{-/-}$) into C57BL/6NCrl mice intravenously. Long-term observation inside a peripheral lymph node was enabled by a novel lymph node internal window chamber technique that allows chronic, sequential lymph node imaging under *in vivo* physiologic conditions. Interestingly, during early stages of tumor progression we found that few if any lymphoma cells homed initially to the inguinal lymph node (ILN), despite clear evidence of lymphoma cells in the bone marrow and spleen. Unexpectedly, we detected a reproducible efflux of lymphoma cells from spleen and bone marrow, concomitant with a massive and synchronous influx of lymphoma cells into the ILN, several days after injection. We confirmed a coordinated efflux/influx of tumor cells by injecting EL-Arf$^{-/-}$ lymphoma cells directly into the spleen and observing a burst of lymphoma cells, validating that the burst originated in organs remote from the lymph nodes. Our findings argue that in NHL an efflux of tumor cells from one disease site to another, distant site in which they become established occurs in discrete bursts. *Cancer Res; 72(23); 6111–8. ©2012 AACR.*

Introduction

Human non-Hodgkin lymphoma (NHL) is a heterogeneous and highly disseminated disease that includes very aggressive subtypes that display explosive growth, such as Burkitt's lymphoma (1). The mechanisms and microscale details of lymphoma growth and dissemination are not yet well understood. Yet such knowledge could greatly improve strategies for early detection and management of patients with lymphoma. Reliable approaches for longitudinal monitoring of lymph nodes in animal models are thus critical to help elucidate biologic phenomena occurring in lymph nodes.

Authors' Affiliations: [1]Molecular Imaging Program at Stanford; [2]Department of Radiology, Stanford University, Stanford, California; [3]Cold Spring Harbor Laboratories, Cold Spring Harbor, New York; [4]Department of Nuclear Medicine & Molecular Imaging, Ajou University School of Medicine, Suwon; and [5]Department of Radiation Oncology, University of Ulsan College of Medicine, Seoul, South Korea

Note: Supplementary data for this article are available at Cancer Research Online (http://cancerres.aacrjournals.org/).

K. Ito and B.R. Smith contributed equally to this work.

Corresponding Author: Sanjiv Sam Gambhir, Departments of Radiology & Bioengineering, Clark Center, East Wing, First Floor E150, 318 Campus Drive East, Stanford, CA 94305. E-mail: sgambhir@stanford.edu

doi: 10.1158/0008-5472.CAN-12-2579

To directly address the mechanisms of lymphoma progression, we focused on the murine inguinal lymph node (ILN) and imaged cancer progression using intravital microscopy (IVM) combined with bioluminescence imaging in living mice. We used the *Eμ-myc* transgenic mouse model, which expresses the *Myc* oncogene in the B-cell compartment, resulting in mice with transplantable lymphomas. This orthotopic mouse lymphoma model was chosen because it captures critical genetic and pathologic features of the human disease (2, 3). IVM has long been a useful tool to address unknown biologic mechanisms in diverse fields including immunology (4–6), cancer biology (7–11), nanoparticle delivery (12–14), drug discovery (15), and biomarker research (16), and so on in animal models. Although lymph nodes have been imaged in mice using IVM for over a decade (17, 18), current techniques to directly and chronically image a lymph node microscopically are still lacking. Because of the lack of a chronic microscale lymph node imaging technique reported in the literature, we established one for the serial visualization of lymphoma development under physiologic conditions and combined it with bioluminescence imaging to reveal the mechanisms by which lymphoma actually forms.

Normal lymphocyte trafficking is essential for the regulation of systemic immune processes, as well as lymphocyte differentiation and development. Most mature lymphocytes recirculate continuously from blood to tissue and back to the blood again (19). This recirculation is regulated by lymphocyte–

endothelial interactions mediated by adhesion molecules (e.g., L-selectin, CD44, integrin, VLA-4, LFA-1) and select chemokines (20, 21). Such interactions may be maintained in lymphoma trafficking patterns; it is believed that unlike the metastasis of other cancers, lymphoma dissemination likely reflects conserved physiologic behavior—normal lymphocyte homing and recirculation molecules have been implicated in lymphoma dissemination and invasion (20, 21). However, the precise mechanisms and time frame of lymphoma trafficking are not well understood. Improved methods and targets for detection and therapy for the disease could likely result from understanding the time course and mechanisms (20, 21), particularly unpredictable characteristics of disease that diverge from normal trafficking patterns.

In this study, we developed a novel lymph node internal window chamber (LNIWC) and with bioluminescence examined lymphoma growth and dissemination in spatial and temporal detail. We made surprising observations that seem to constitute processes distinct from normal lymphocyte homing patterns: for instance, within a 12-hr period identified via chronic serial imaging, we reproducibly observed a large, rapid efflux from the bone marrow and spleen, with a concomitant influx of lymphoma cells into the ILN region.

Materials and Methods

Cell culture

Eμ-myc/Arf$^{-/-}$ lymphoma cells that harbor loss-of-function regions in the *Arf* gene were derived by intercrossing *Eμ-myc* transgenic mice with *Arf*-null mice, all in the C57BL/6 background as described previously (2). *Eμ-myc/Arf*$^{-/-}$ lymphoma cells and EL-Arf$^{-/-}$ lymphoma cells were cultured in a mixed medium including Dulbecco's Modified Eagle's Medium and Iscove's Modified Dulbecco's Medium with 10% FBS and 1% penicillin G-streptomycin on irradiated mouse embryonic fibroblast feeder cells. *Eμ-myc/Arf*$^{-/-}$ and *Eμ-myc/p53*$^{-/-}$ cells were obtained from Dr. Scott Lowe's Laboratory (Cold Spring Harbor, NY) in 2009. These cell lines were authenticated, showing that the *Arf* and *p53* genes were deleted, respectively, and that these murine cells overexpress the myc gene. PCR was used for detection with a specific primer. In 2010, we confirmed that the *Arf*$^{-/-}$ gene is deleted using PCR. Also in 2010, we confirmed that either Arf or p53 was deleted in the respective cell lines via Western blotting.

Lentiviral reporter gene construct

Firefly luciferase (Luc2)-eGFP, linked by gcctctgctg-cctctgcc that encodes 6 amino acids (VSAVSA), was kindly provided by Dr. Christopher Contag (Stanford University, Stanford, CA). This vector contains the Ubiquitin C promoter sequence. The details can be found in the Supplementary Methods.

Murine lymphoma model

C57BL/6 mice were purchased from Charles River Laboratories (Wilmington, MA). All animal studies were approved by The Stanford University Institutional Animal Care and Use Committee. A total of 1×10^6 EL-Arf$^{-/-}$ Lymphoma cells were diluted with 200 μL of PBS and injected intravenously via the tail vein as described (2). Control mice were injected with 200 μL of PBS.

Internal window chamber implantation

Animals were anesthetized with isoflurane, hair was removed from mice using hair clippers and depilatory cream. An incision was made on the peritoneal skin and the left ILN was located on the internal side of the mouse skin by reference to the intersection of 3 large blood vessels on the interior after the tissue has been opened (see Fig. 1C). From the interior, our

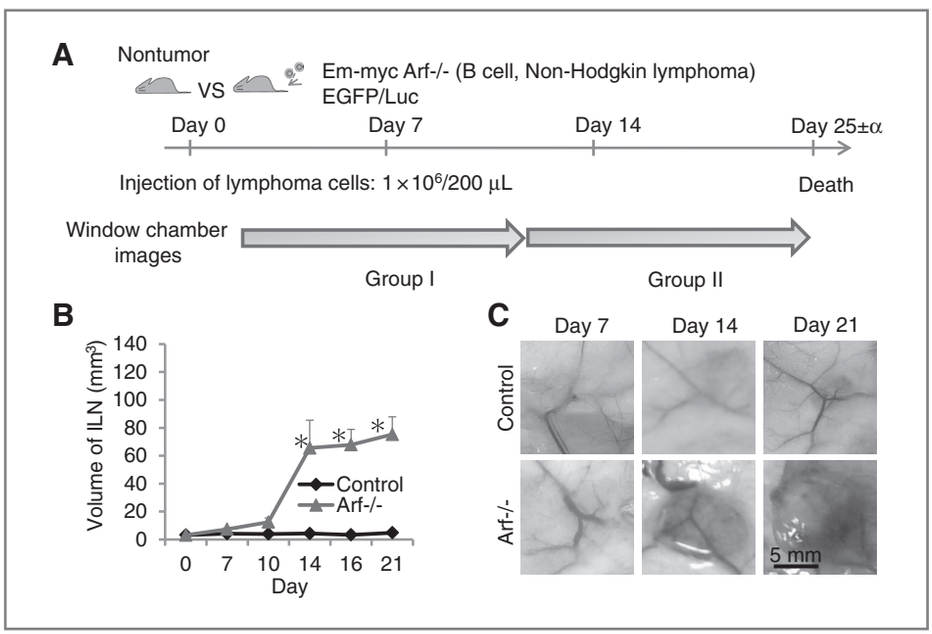

Figure 1. Mouse lymphoma model. A, EL-Arf$^{-/-}$ cells (1×10^6) were tail-vein injected into C57BL/6 mice. LNIWC imaging was separated into 2 groups: group I was focused on from day 0 to 10, and for group II from day 11 to 17. This was done because of the limitation of repeatedly opening the staples up to 6 to 7 times in the same mouse. $N = 7$ mice were imaged with IVM in each group in 6 independent experiments. B, tumor development in the ILN. Symbols represent the means of ILN volumes determined by $N = 3$ to 7 animals for each point. Bars, SEM; *, $P < 0.05$. C, representative images of the ILN on days 7, 14, and 21 postinjection.

custom-made titanium frames were placed onto the ILN region and fixed in place using surgical sutures (Blue Polypropylene, 5-0, FS-2; Med Rep Express). Thus, this window chamber resides within the living animal with tissues above and surrounding it in this novel strategy. The skin was closed with surgical staples (Braintree Scientific, Inc.). The details of the surgical procedure can be viewed online (Supplementary Movie S1).

Intravital microscopy

Images were collected with an intravital laser-scanning microscope (IV-100; Olympus Corporation) using Olympus UplanFL objectives and Olympus FluoView FV300 version 4.3 software. ImageJ (NIH) and Olympus software was used for image processing. Regions of the lymph nodes were excited with a set of lasers at 488 and 748 nm to detect EL-Arf$^{-/-}$ lymphoma cells and outline the blood vessels. The details can be found in the Supplementary Methods.

Bioluminescence imaging

For bioluminescence imaging, 0.2 mL of 15 mg/mL D-luciferin (Biosynth AG) was injected intraperitoneally into C57BL/6 mice under 1% to 2% inhaled isoflurane anesthesia. Bioluminescence signal was monitored using the IVIS system 200 series (Xenogen), consisting of a highly sensitive, cooled charge-coupled device camera. Living Image software (Xenogen) was used to grid the imaging data and integrate the total bioluminescence signal in each region-of-interest (ROI). All bioluminescence images were acquired with a 1 second exposure. Data were analyzed using total photon flux emission (photons/second) in the ROIs. Data were normalized using the background signal.

Analysis of enhanced green fluorescent protein positive cells

To assess enhanced green fluorescent protein (EGFP)+ cells in murine tissues, the bone marrow, ILN, and spleen were isolated from C57BL/6 mice on day 7 and 14 after EL-Arf$^{-/-}$ cell inoculation. All tissues were minced and filtered with a 100 μm cell strainer (BD Falcon). The cells were analyzed by a FACScan flow cytometer (Becton Dickinson).

Statistical analysis

Results were expressed as mean ± SEM. An unpaired, 2-tailed Student t test was used to calculate P values (except for Fig. 2D, in which a Wilcoxon test was used). P values of 0.05 or less were considered statistically significant.

Results

Eμ-myc Arf$^{-/-}$ lymphoma mouse model

To image and analyze lymphoma development in detail, we applied a multimodal intravital fluorescence and bioluminescence imaging approach to an established lymphoma model (2) by transfecting a lentiviral vector containing firefly luciferase and EGFP sequences into the parental (*Eμ-myc/Arf*$^{-/-}$ cells) line to generate EGFP/luc2 (EL-Arf$^{-/-}$) cells. To ensure that expression of firefly luciferase and EGFP protein does not induce abnormal biologic function, we compared the cell growth patterns and the apoptosis sensitivity between the parental (*Eμ-myc/Arf*$^{-/-}$ cells) and the lentivirus-transfected lymphoma cells (EL-Arf$^{-/-}$ cells). We confirmed there is no significant difference in cell growth and apoptosis sensitivity between the 2 sets of cells (Supplementary Fig. S1), which indicates that the reporter genes we inserted do not modify these lymphoma cell properties; furthermore, our results are consistent with results generated from the parental cell line (2, 22).

Previous studies on this lymphoma model have not elucidated tumor and angiogenesis development in the ILN. In initial experiments, we analyzed tumor development patterns using isosulfan blue to localize the lymph node and analyzed angiogenesis development using IVM. With IVM, we identified that microvascular number and circulating dye intensity was significantly higher in EL-Arf$^{-/-}$ lymphoma cell injected-mice compared with control mice from day 14 onward (Supplementary Fig. S2). Using macroscopic observation, we observed significant tumor development after day 14 compared with PBS-injected control mice ($P < 0.05$; Fig. 1B and C).

In the early-stage EL-Arf$^{-/-}$ lymphoma cells expand in the bone marrow and spleen but not ILN

To understand cell proliferation patterns in mice at the whole-body level, we conducted frequent (daily) bioluminescence imaging on living mice ($N = 12$ per group) after injection of either EL-Arf$^{-/-}$ cells or PBS. On day 7 (and earlier), we detected bioluminescence signal in the bone marrow and spleen but not in the ILN (Fig. 2A). We conducted further analysis to validate our imaging results: we isolated the bone marrow, ILN, and spleen from mice 7 days after EL-Arf$^{-/-}$ lymphoma cell or PBS injection, then the EGFP+ cell population was analyzed using flow cytometry. We detected a significant number of EGFP+ cells in the bone marrow and spleen, but not in the ILN (Fig. 2B and C). PCR data also showed that less than 100 EL-Arf$^{-/-}$ lymphoma cells (if any) are located in the ILN by day 3 (Fig. 2D). Furthermore, we confirmed these results using *ex vivo* bioluminescence analysis on days 7 and 14 (Supplementary Fig. S3). These data collectively indicate that EL-Arf$^{-/-}$ cells proliferated in both the bone marrow and the spleen, but not in the ILN in the early stage of cancer progression.

Efflux of EL-Arf$^{-/-}$ lymphoma cells from the bone marrow and spleen to the periphery in the middle stage

In the early stage of lymphoma dissemination, frequent bioluminescence imaging displayed an increasing signal in the bone marrow and spleen (i.e., proliferation of EL-Arf$^{-/-}$ cells) but not the ILN. Yet interestingly, toward the middle stage (after day 8), we observed decreased bioluminescence signal in the bone marrow (66.5 ± 8.7, day 8 vs. day 8.5) and spleen (36.0 ± 3.6, day 8 vs. day 8.5) with a concomitant increase in signal in the ILN (215.0 ± 57.0, day 8 vs. day 9; $N = 12$ EL-Arf$^{-/-}$ injected group, $N = 5$ control mice; Fig. 3A and B). The phenomenon observed is thus highly reproducible

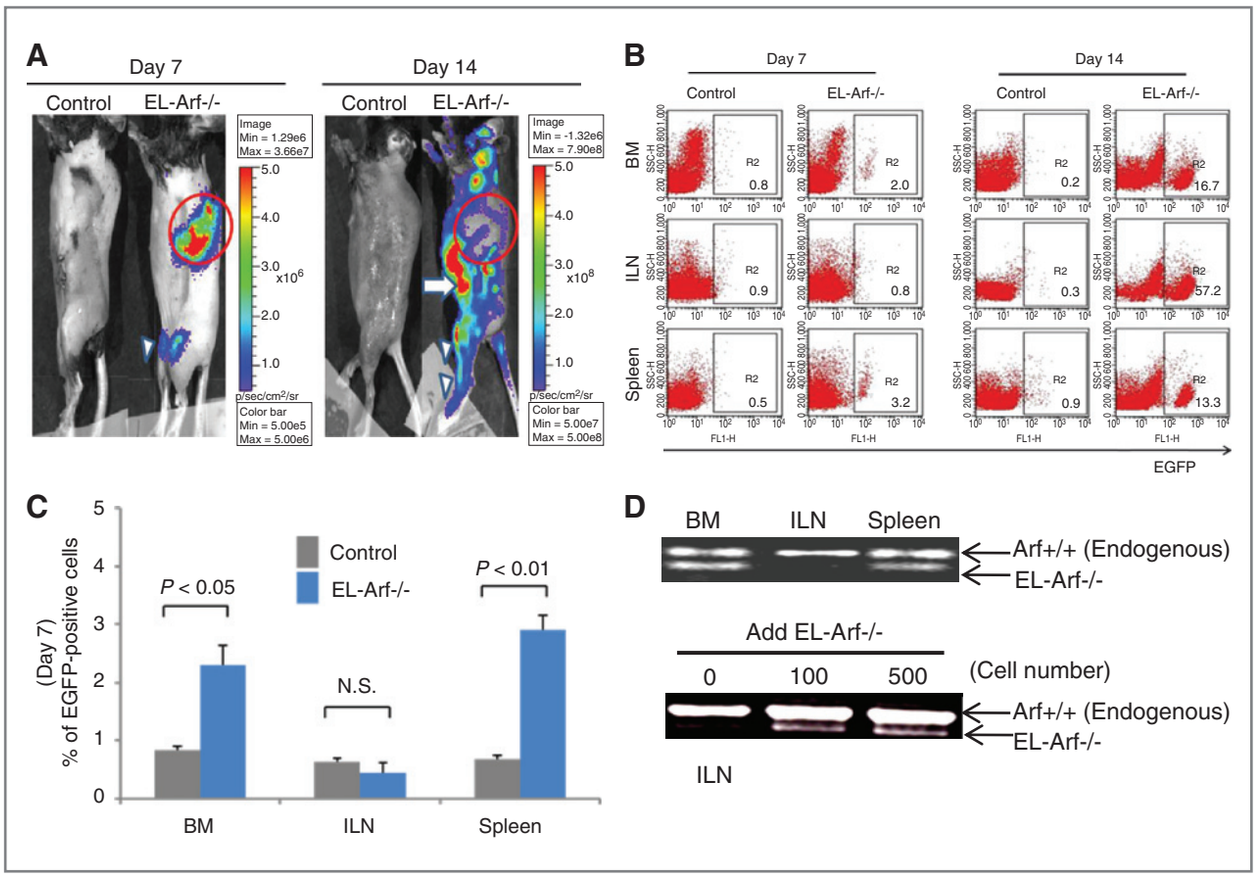

Figure 2. Lymphoma cells proliferate in the bone marrow (BM) and spleen but not in the ILN node in the early stage. Bioluminescence images were acquired after injection of EL-Arf$^{-/-}$ cells or control. A, bioluminescence images are shown on days 7 and 14. The arrow designates the ILN, which is visible with bioluminescence by day 14. The arrowhead shows bone marrow (femur) and the red circle indicates spleen ($N = 10$ each group). B and C, EGFP+ cell analysis using FACS. B, representative FACS dot plot of EGFP+ cells in bone marrow, spleen, and ILN on days 7 and 14 after injection. C, the columns represent the means of percentages of EGFP+ cells from 3 independent experiments ($N = 8$ each group). Bars, SEM; *, $P < 0.05$. D, expression analysis of EL-Arf$^{-/-}$ lymphoma cells in mouse inguinal lymph node using highly sensitive PCR on day 3. Top, either Arf$^{+/+}$ (endogenous normal cells) or EL-Arf$^{-/-}$ lymphoma cell expression pattern; bottom, quantitative PCR. The indicated EL-Arf$^{-/-}$ cell number was exogenously added into the ILN directly, showing that although we can detect as few as 100 EL-Arf$^{-/-}$ cells in the ILN, no lymphoma cells are detectable in an EL-Arf$^{-/-}$ injected mouse on day 3 ($N = 3$, carried out more than 3 independent experiments).

and the timepoint at which it occurs postinjection is rather specific. Moreover, when we increased the initial injection cell number 5-fold (to 5×10^6 EL-Arf$^{-/-}$ cells), we reproducibly observed a much earlier efflux of EL-Arf$^{-/-}$ lymphoma cells around day 5 (Supplementary Fig. S4). This result may reveal a dependence of the efflux on local cell concentration. Furthermore, even when injecting EL-Arf$^{-/-}$ lymphoma cells directly into the spleen (rather than via tail vein, so that no cells could have initially seeded the periphery), importantly we observed the same phenomenon: efflux from spleen and influx to ILN (Supplementary Fig. S5). These results strongly indicate that EL-Arf$^{-/-}$ lymphoma cells proliferate in the spleen and bone marrow, then flow out from these sites to the periphery. Importantly, we also observed the same efflux/influx phenomenon using a different lymphoma cell type (p53$^{-/-}$ crossed with *Eμ-myc* and transfected with EGFP/luc2, termed EL-p53$^{-/-}$) via bioluminescence imaging (Supplementary Fig. S6).

Sudden, huge influx of the lymphoma cells into peripheral lymph node

To sequentially image the genesis of lymphoma in the ILN at the microscale, we developed a novel LNIWC. It consisted of a titanium frame (9.0 mm diameter, 2.0 mm thickness, and 0.35 g). An incision was made on the peritoneal skin, and the ILN was located visually by the vascular pattern (Supplementary Movie S1). The LNIWC was then implanted over the ILN. The LNIWC was fixed in place with sutures and the peritoneal region was closed with surgical clips (Fig. 4A–C and Supplementary Movie S1). Surgical clips were removed and access to the window was obtained every time IVM was conducted, then the clips were replaced each time. This approach enables us to serially obtain IVM images for up to 2 weeks, and we validated the technique's use against 2 other methods for visualizing the ILN sequentially on the microscale (see Supplementary Table S1). These 2 other methods are similar to techniques that have been used for imaging other abdominal organs, such as

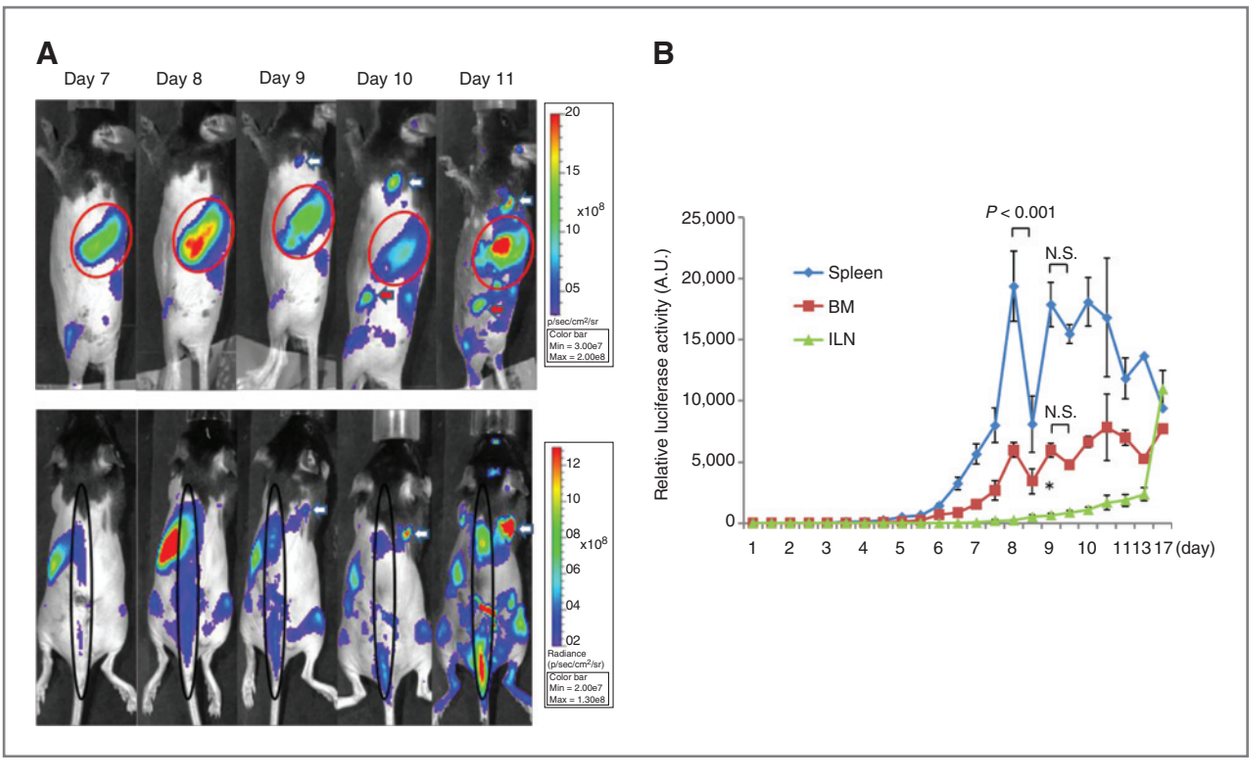

Figure 3. Efflux of lymphoma cells from the spleen and bone marrow to the periphery in the middle stage. A, representative bioluminescence images (from $N = 12$ mice) in an EL-Arf$^{-/-}$ cell–injected mouse. Top, mice placed on their side; the red arrow indicates the ILN and the white arrow indicates a superficial cervical lymph node. The red circle designates the spleen. The bottom displays prone images; the black ellipse designates the bone marrow and the white arrow indicates a superficial cervical lymph node. B, average bioluminescence signal from the bone marrow, ILN, and spleen over time. Each point represents the bioluminescence signal from 7 to 12 mice in 4 independent experiments. *, $P < 0.05$. Bars, SEM. BM, bone marrow; N.S., not significant.

liver and other "body windows," but they suffered from difficulties due primarily to the unique challenges of serially imaging the lymph node in living subjects (as a result of the intimate vascular connections between lymph node and adjacent tissue, these techniques suffered from tissue adhesions and fibrosis, see Supplementary Information). We chose to use the LNIWC method in our experiments due to its ability to considerably decrease autofluorescence in serial imaging

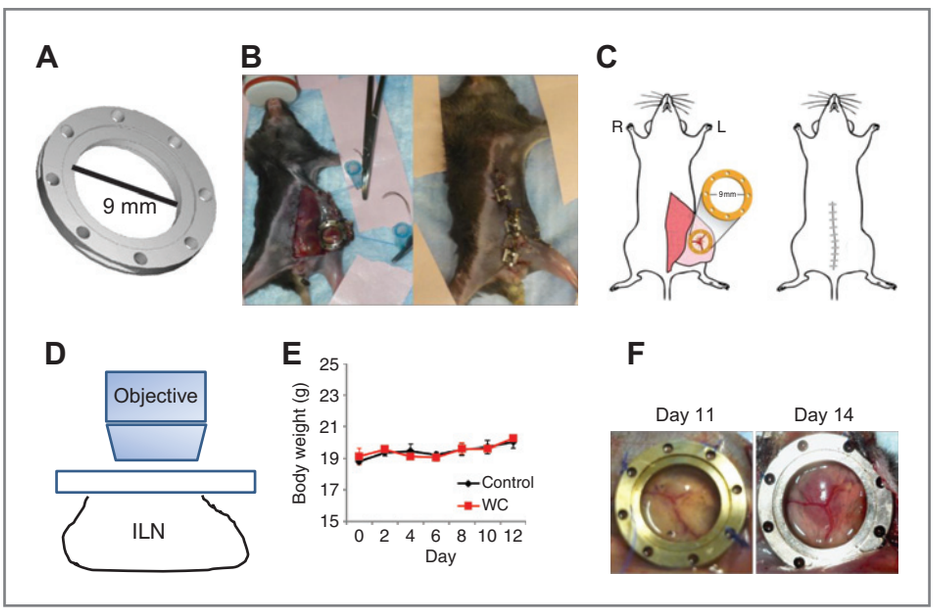

Figure 4. Development of the lymph node window chamber technique. A, schematic of the titanium lymph node window chamber. B, representative picture of a mouse after implantation of the LNIWC over the mouse ILN (left). The surgical clips are used to close the skin until the next imaging session (right). C, schematic of the placement of the LNIWC after surgical implantation (left) over the ILN, and a schematic of the mouse after closing the skin using surgical clips (right). D, schematic of IVM being conducted using the LNIWC. E, body weight measurements of C57BL/6 mice either carrying the LNIWC (WC) or not (control). Symbols represent the means of body weight. $N = 3$ mice per group in a single independent experiment. Bars, SEM. F, representative pictures of tumor growth in the LNIWC.

sessions and because it provided a fiduciary marker for us to consistently return to precisely the same sites to image them longitudinally (see Supplementary Information). We observed neither loss in body weight ($P = 0.67$) nor any unusual mouse behavior throughout the observation period in both the LNIWC and non-LNIWC groups (Fig. 4E, Supplementary Movie S2). We were also able to observe macroscopic tumor growth in the LNIWC (Fig. 4F). In accordance with our PCR and bioluminescence data, we were unable to detect EGFP-expressing cells in the ILN until day 9.1 after injection of the EL-Arf$^{-/-}$ cell group ($N = 7$ mice) using IVM; however, we never detected EGFP signal from the control (PBS-injected) mice ($N = 4$; Fig. 5A and B, Supplementary Fig. S7). We also observed the same reproducible phenomena in our other lymphoma model, the EL-p53$^{-/-}$ injected mice, using IVM (Supplementary Fig. S8). Furthermore, using the LNIWC with IVM high-resolution imaging, we observed a single circulating EL-Arf$^{-/-}$ lymphoma cell in the vasculature feeding the ILN on day 10 (Supplementary Movie S3), although we never observed tumor cells in vasculature on other days. This suggests that effluxed lymphoma cells likely reach and seed the periphery via blood circulation. Fluorescence-activated cell sorting (FACS) and PCR analyses validated that no tumor cells were present in ILN both 3 days and 1 week after EL-Arf$^{-/-}$ injection (Fig. 2B–D). Because we were able to image the same mouse at the same site every 2 to 3 days, we observed a relatively sudden EL-Arf$^{-/-}$ cell influx into the ILN between day 8 to 10 postinjection. To focus on this time period, we obtained IVM-images

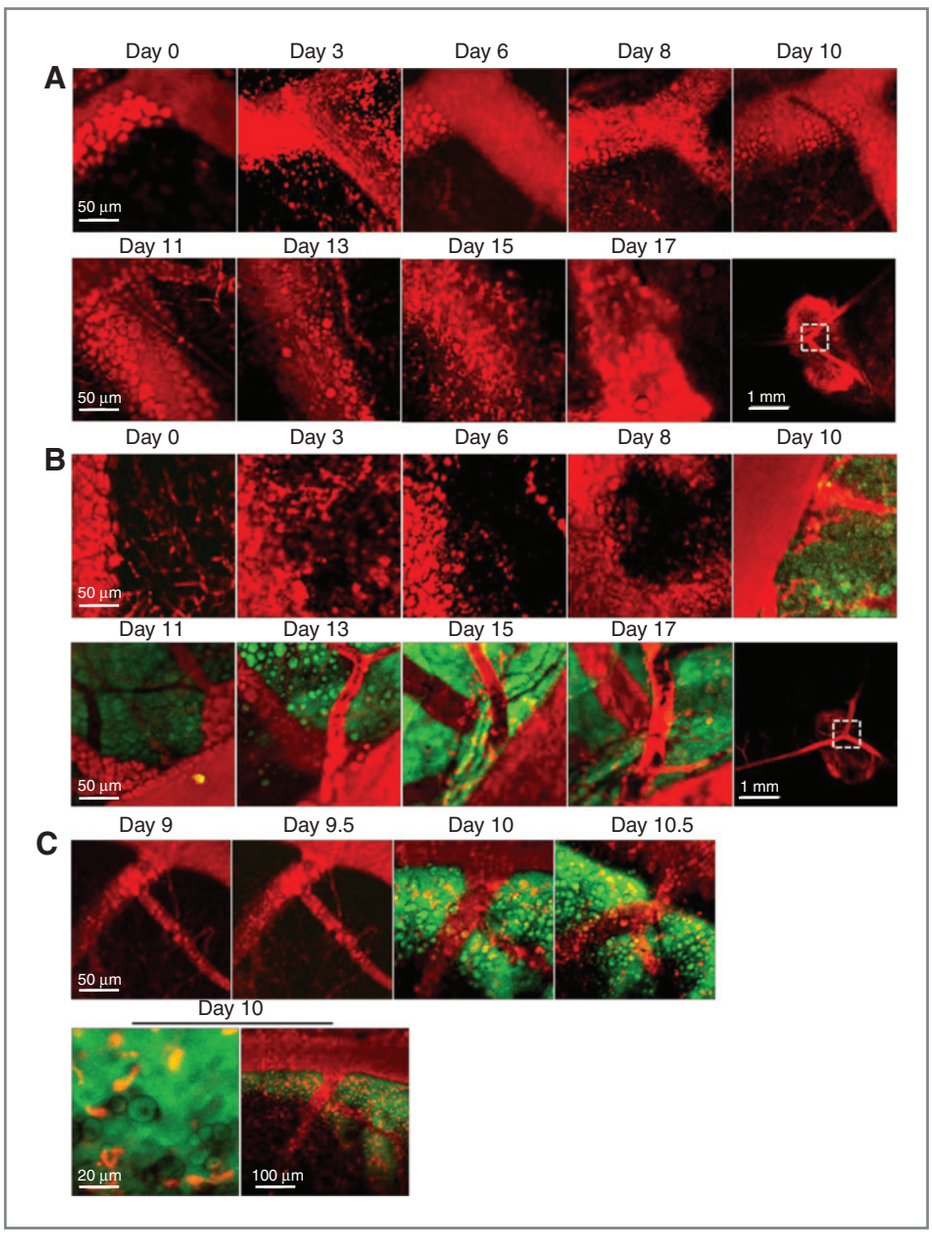

Figure 5. Lymph node internal window chamber images. A, control mouse images from day 0 to 17. The final panel represents the larger-scale region that was imaged. B, IVM imaging of EL-Arf$^{-/-}$ cell–injected mice. C, high-temporal resolution images obtained twice daily of EL-Arf$^{-/-}$ cell–injected mice. Red, blood vessels (via dye) and adipocytes (by autofluorescence). Green, EL-Arf$^{-/-}$ cells. Yellow, merged green/red regions. We validated these data in $N = 7$ mice per group, with the experiment carried out independently 6 times.

every 12 hours from 8 to 10 days postinjection of cells. Intriguingly, we observed a sudden large influx of EL-Arf$^{-/-}$ cells into the ILN within a 12-hour time period reproducibly across $N = 7$ mice (Fig. 5B and C). Therefore, the LNIWC, which has not been previously described for intravital imaging, enabled us to visualize the ILN longitudinally and observe the "burst effect" of cells into the ILN.

Using immunohistochemistry we then showed that after these cells arrive, the EL-Arf$^{-/-}$ lymphoma cells establish a rapidly proliferating tumor in the ILN (Supplementary Fig. S9). These results together indicate that EL-Arf$^{-/-}$ lymphoma cells flow out from the spleen/bone marrow to the periphery via the circulation in the middle stage and then proliferate to form a tumor in peripheral lymph nodes (including the ILN and superficial cervical lymph nodes, see Fig. 3). Furthermore, these results suggest the spleen must be somehow conditioned for efflux and underscore the use of multimodal IVM and bioluminescence imaging to visualize tumor cell trafficking in live mice.

Discussion

Malignant transformation of normal lymphocytes results in lymphoma, and many lymphoma subtypes migrate and disseminate. This dissemination may reflect conserved physiologic behavior unlike the metastasis of other cancers, considering that normal lymphocyte homing and recirculation molecules have been implicated in lymphoma dissemination and invasion. Because the time course and mechanisms of lymphoma trafficking are not well understood, we developed a multimodal imaging platform to sequentially image lymphoma cells; we combined a novel LNIWC technique for IVM with bioluminescence imaging to derive time course and basic mechanistic information on lymphoma development.

The LNIWC, which represents a modification of previous window chamber techniques (23), was developed to obtain sequential images. The LNIWC method can be used to serially image (up to 2 weeks for 6–7 independent imaging sessions) the ILN to observe lymphoma progression in an orthotopic mouse lymphoma model under physiologic conditions. Critically, the method also enabled us to easily find and image the same location during each imaging session because of the ability to use the LNIWC as a spatial point-of-reference, including suture holes and the chamber itself for spatial orientation. To our knowledge, this technique enables the first instance of serial imaging of a lymph node in a living mouse.

Using multimodal (intravital/bioluminescence) imaging, we discovered a key, novel feature of the EL-Arf$^{-/-}$ lymphoma model: tumor cell initiation and expansion in the bone marrow and spleen, followed by a burst into peripheral lymph nodes and progression in the ILN. It is notable that this cell line is not unique in this respect—we observed that the EL-p53$^{-/-}$ cell line also displayed a similar, reproducible pattern of efflux/influx (Supplementary Figs. S6 and S8), suggesting the mechanism we observed is not model dependent and is likely to be a more general feature of lymphoma dissemination. The insights achieved with these models could prove invaluable in understanding how different genetic alterations can influence migration of lymphoid cells to different lymphoid sites as these models are in many ways similar to human lymphoma (2, 3).

We note that before this work, the lymph node tumors in these murine models were evaluated primarily via palpation and whole-body fluorescence imaging, which are not sensitive to low numbers of tumor cells and thus do not provide detailed information particularly at the earlier time points. Therefore, it was previously presumed that in the *Eμ-myc* lymphoma model tumors began forming within the lymph node immediately after the intravenous injection of cells (2). Given the previous assumptions, we were initially surprised to find a lack of lymphoma cells in the ILN during the first approximately 9 days after injection using IVM. Our findings using the LNIWC, which were further validated by bioluminescence, FACS, and PCR analyses, collectively show that around day 9 tumor cells exit the spleen and bone marrow and at least some fraction of these cells very reproducibly and robustly reach the ILN. It was surprising to us that lymphoma cells do not gradually depart from the spleen and bone marrow into the ILN, but instead they arrive rapidly in a burst into the ILN. Although the murine lymphoma model differs in several aspects from human lymphoma, our preclinical findings do mirror distribution patterns in human lymphoma such as splenic marginal zone lymphoma and chronic lymphocytic leukemia in the later stages. Early in these diseases, lymphoma cells appear in the bone marrow and spleen, without significant peripheral node involvement. In later stages, lymphoma cells can often be found in other organs (24–27) with increasing tumor burden and even after successful treatment, lymphoma cells may "reseed" the original lymph nodes/lymphoma (28). This reseeding can critically accelerate tumor growth, angiogenesis, and the recruitment of stromal elements (28). Our model may be applicable to these and other NHL, in which the bone marrow and spleen could serve as reservoirs for cells that seed and reseed recurrent sites of disease. Understanding the pattern and mechanisms of lymphoma progression could unlock new ways to detect and treat this disease. More generally, our model may help answer key questions about the interplay of host factors and microenvironment that allow malignant cells to home to, proliferate at, and exit from specific sites of disease in a wide range of hematologic and solid tumors. Therefore, with the advent of biologic therapies and immune modulation for treatment of cancer, understanding what triggers this efflux, and critically finding ways to delay or even stop it, may enable physicians to interfere with disease spreading, reseeding, or further metastasizing.

In conclusion, our multimodal intravital (LNIWC) and bioluminescence approach enabled us to explore how a lymphoma mass truly evolves within the lymph node; this led us to discover lymphoma cell efflux from the spleen and bone marrow and a concomitant influx into the ILN within a surprisingly short time period. This finding has implications for understanding and developing novel treatment regimens for human lymphoma and potentially other cancers.

Disclosure of Potential Conflicts of Interest

No potential conflicts of interest were disclosed.

Authors' Contributions

Conception and design: K. Ito, B.R. Smith, P. Mallick, S.W. Lowe, S.S. Gambhir
Development of methodology: K. Ito, B.R. Smith, N. Parashurama, J.-K. Yoon, S. Y. Song
Acquisition of data (provided animals, acquired and managed patients, provided facilities, etc.): K. Ito, B.R. Smith, J.-K. Yoon, S.Y. Song, C. Miething, S. W. Lowe
Analysis and interpretation of data (e.g., statistical analysis, biostatistics, computational analysis): K. Ito, B.R. Smith, N. Parashurama, J.-K. Yoon, C. Miething, S.S. Gambhir
Writing, review, and/or revision of the manuscript: K. Ito, B.R. Smith, N. Parashurama, P. Mallick, S.W. Lowe, S.S. Gambhir
Administrative, technical, or material support (i.e., reporting or organizing data, constructing databases): K. Ito, B.R. Smith, S.S. Gambhir
Study supervision: B.R. Smith, P. Mallick, S.S. Gambhir

Acknowledgments

The authors thank Drs. Alice Fan and Laurence Marton for their assistance in article review. The authors are also grateful to Prof. Chen Yuan Dong for discussions on window chambers.

Grant Support

This work was supported in part by NCI PS-OC MC-START U54 CA143907 and NCI U54 CA119367.

The costs of publication of this article were defrayed in part by the payment of page charges. This article must therefore be hereby marked *advertisement* in accordance with 18 U.S.C. Section 1734 solely to indicate this fact.

Received June 29, 2012; revised August 31, 2012; accepted September 18, 2012; published OnlineFirst October 2, 2012.

References

1. Lenz G, Staudt LM. Aggressive lymphomas. N Engl J Med 2010; 362:1417–29.
2. Schmitt CA, Fridman JS, Yang M, Lee S, Baranov E, Hoffman RM, et al. A senescence program controlled by p53 and p16INK4a contributes to the outcome of cancer therapy. Cell 2002;109:335–46.
3. Lowe SW, Sherr CJ. Tumor suppression by Ink4a-Arf: progress and puzzles. Curr Opin Genet Dev 2003;13:77–83.
4. Swirski FK, Nahrendorf M, Etzrodt M, Wildgruber M, Cortez-Retamozo V, Panizzi P, et al. Identification of splenic reservoir monocytes and their deployment to inflammatory sites. Science 2009;325:612–6.
5. Deguine J, Breart B, Lemaitre F, Di Santo JP, Bousso P. Intravital imaging reveals distinct dynamics for natural killer and CD8(+) T cells during tumor regression. Immunity 2010;33:632–44.
6. Mempel TR, Pittet MJ, Khazaie K, Weninger W, Weissleder R, von Boehmer H, et al. Regulatory T cells reversibly suppress cytotoxic T cell function independent of effector differentiation. Immunity 2006; 25:129–41.
7. Yang M, Jiang P, Hoffman RM. Whole-body subcellular multicolor imaging of tumor-host interaction and drug response in real time. Cancer Res 2007;67:5195–200.
8. Yang M, Baranov E, Wang JW, Jiang P, Wang X, Sun FX, et al. Direct external imaging of nascent cancer, tumor progression, angiogenesis, and metastasis on internal organs in the fluorescent orthotopic model. Proc Natl Acad Sci U S A 2002;99:3824–9.
9. Kedrin D, Gligorijevic B, Wyckoff J, Verkhusha VV, Condeelis J, Segall JE, et al. Intravital imaging of metastatic behavior through a mammary imaging window. Nat Methods 2008;5:1019–21.
10. Fukumura D, Duda DG, Munn LL, Jain RK. Tumor microvasculature and microenvironment: novel insights through intravital imaging in preclinical models. Microcirculation 2010;17:206–25.
11. Lohela M, Werb Z. Intravital imaging of stromal cell dynamics in tumors. Curr Opin Genet Dev 2010;20:72–8.
12. Smith BR, Cheng Z, De A, Koh AL, Sinclair R, Gambhir SS. Real-time intravital imaging of RGD-quantum dot binding to luminal endothelium in mouse tumor neovasculature. Nano Lett 2008;8:2599–606.
13. Smith BR, Cheng Z, De A, Rosenberg J, Gambhir SS. Dynamic visualization of RGD-quantum dot binding to tumor neovasculature and extravasation in multiple living mouse models using intravital microscopy. Small 2010;6:2222–9.
14. Smith BR, Kempen P, Bouley D, Xu A, Liu Z, Melosh N, et al. Shape matters: intravital microscopy reveals surprising geometrical dependence for nanoparticles in tumor models of extravasation. Nano Lett 2012;12:3369–77.
15. Miyazaki J, Tsuzuki Y, Matsuzaki K, Hokari R, Okada Y, Kawaguchi A, et al. Combination therapy with tumor-lysate pulsed dendritic cells and antiangiogenic drug TNP-470 for mouse pancreatic cancer. Int J Cancer 2005;117:499–505.
16. Arad A, Proulle V, Furie RA, Furie BC, Furie B. β2-Glycoprotein-1 autoantibodies from patients with antiphospholipid syndrome are sufficient to potentiate arterial thrombus formation in a mouse model. Blood 2011;24:3453–9.
17. von Andrian UH. Intravital microscopy of the peripheral lymph node microcirculation in mice. Microcirculation 1996;3:287–300.
18. Diacovo TG, Puri KD, Warnock RA, Springer TA, von Andrian UH. Platelet-mediated lymphocyte delivery to high endothelial venules. Science 1996;273:252–5.
19. Gowans JL. Life-span, recirculation, and transformation of lymphocytes. Int Rev Exp Pathol 1966;5:1–24.
20. Gallatin M, St John TP, Siegelman M, Reichert R, Butcher EC, Weissman IL. Lymphocyte homing receptors. Cell 1986;44:673–80.
21. Pals ST, de Gorter DJ, Spaargaren M. Lymphoma dissemination: the other face of lymphocyte homing. Blood 2007;110:3102–11.
22. Schmitt CA, McCurrach ME, de Stanchina E, Wallace-Brodeur RR, Lowe SW. INK4a/ARF mutations accelerate lymphomagenesis and promote chemoresistance by disabling p53. Genes Dev 1999;13: 2670–7.
23. Bertera S, Geng X, Tawadrous Z, Bottino R, Balamurugan AN, Rudert WA, et al. Body window-enabled *in vivo* multicolor imaging of transplanted mouse islets expressing an insulin-Timer fusion protein. Biotechniques 2003;35:718–22.
24. Matutes E, Oscier D, Montalban C, Berger F, Callet-Bauchu E, Dogan A, et al. Splenic marginal zone lymphoma proposals for a revision of diagnostic, staging and therapeutic criteria. Leukemia 2008;22: 487–95.
25. Mazloom A, Rodriguez A, Ha CS, Medeiros LJ, Wogan C, Shihadeh F, et al. Incidence of gastric involvement in patients with nongastrointestinal extranodal marginal zone lymphoma. Cancer 2011;117: 2461–6.
26. Mollejo M, Lloret E, Menarguez J, Piris MA, Isaacson PG. Lymph node involvement by splenic marginal zone lymphoma: morphological and immunohistochemical features. Am J Surg Pathol 1997;21:772–80.
27. Ghia P, Ferreri AM, Caligaris-Cappio F. Chronic lymphocytic leukemia. Crit Rev Oncol Hematol 2007;64:234–46.
28. Kim MY, Oskarsson T, Acharyya S, Nguyen DX, Zhang XH, Norton L, et al. Tumor self-seeding by circulating cancer cells. Cell 2009;139: 1315–26.